A simplified approach to evaluating slope stability under freezing–thawing cycles in soft soils

Ayman Abed[1*]

[1] Department of Architecture and Civil Engineering, Chalmers University of Technology, Sweden

1 Introduction

The stability of natural slopes in soft soil formations is strongly influenced by freezing–thawing cycles, a phenomenon often associated with slope failures in Sweden. Despite numerous documented cases, reliably estimating the safety factor for slopes exposed to such environmental loading remains a challenge. This study addresses this gap by proposing a simplified method for assessing slope stability under freezing–thawing cycles.

The procedure combines finite element (FE) calculations with limit equilibrium analysis (LEM). Results from a fully coupled Thermo–Hydro–Mechanical (THM) finite element model provide a realistic stress field and ice content distribution, which are subsequently used as input for a classical stress-based limit equilibrium analysis. This study represents an initial evaluation of the procedure's capabilities and limitations and concludes by outlining directions for its future refinement.

2 Balance equations used in the THM framework

2.1 Water mass balance equation

The mass balance equation of water in the frozen soil can be written as [1]:

$$\frac{\partial(nS_{rw}\rho_w)}{\partial t}+\frac{\partial(nS_{ice}\rho_{ice})}{\partial t}+\nabla\cdot(nS_{rw}\rho_w v_w)+\nabla\cdot(nS_{ice}\rho_{ice}v_{ice})=0 \tag{1}$$

where n, S_{rw}, ρ_w and v_w are the soil porosity, degree of liquid water saturation, water density and the velocity of liquid water phase, respectively. Similar symbols are used for the ice phase but with the indices ice instead.

After appropriate mathematical manipulation, the above equation yields:

$$\begin{aligned}(S_{rw}\rho_w+S_{ice}\rho_{ice})\frac{\partial\varepsilon_v}{\partial t}+n(\rho_w-\rho_{ice})\frac{\partial S_{rw}}{\partial s_c}\frac{\partial s_c}{\partial T}\frac{\partial T}{\partial t}+n(\rho_w-\rho_{ice})\frac{\partial S_{rw}}{\partial s_c}\frac{\partial s_c}{\partial p_w}\frac{\partial p_w}{\partial t}\\+nS_{rw}\rho_w\beta_w\frac{\partial p_w}{\partial t}-nS_{rw}\rho_w\beta_{wT}\frac{\partial T}{\partial t}+\rho_w\nabla\cdot q_w=0\end{aligned} \tag{2}$$

The symbols ε_v, T, β_w and β_{wT} denote the volumetric strain, temperature in Kelvin, water compressibility and thermal expansion of water, respectively. The cryogenic suction s_c in the equation is defined as the difference between the ice pressure p_{ice} and the porewater pressure p_w. According to Clausius-Clapeyron equation, s_c can be estimate as:

$$s_c=\left(\frac{\rho_{ice}}{\rho_w}-1\right)p_w-L\rho_{ice}\ln\left(\frac{T}{T_0}\right)\approx-L\rho_{ice}\ln\left(\frac{T}{T_0}\right) \tag{3}$$

where L is the latent heat fusion of ice and T_0 is freezing point of water, assumed to be 273.15 K in this study. This equation then allows the calculation of the derivatives in Equation (2):

$$\frac{\partial s_c}{\partial p_w}=\left(\frac{\rho_{ice}}{\rho_w}-1\right)\approx 0;\ \frac{\partial s_c}{\partial T}=-\frac{L\rho_{ice}}{T} \tag{4}$$

Note that the influence of variations in liquid water pressure on the cryogenic suction is negligible compared to the effect of temperature variation and is therefore neglected here.

The liquid water flow is assumed to obey Darcy's law, and the water discharge q_w is thus given as follows:

$$q_w=-\frac{K_w}{\rho_w g}(\nabla p_w+\rho_w g) \tag{5}$$

The most important aspect here is that the hydraulic conductivity of liquid (unfrozen) water K_w is a function of the degree of saturation of unfrozen water S_{rw} which, in turn, depends on the cryogenic suction s_c and is assumed to be described by a pseudo–van Genuchten–Mualem formulation [2]:

$$S_{rw}=S_{res}+(S_{sat}-S_{res})[1+(g_\alpha s_c)^{g_n}]^{g_c} \tag{6}$$

and

* Corresponding author: ayman.abed@chalmers.se

$$K_w = K_{sat} S_e^{g_l} \left[1 - \left(1 - S_e^{\frac{1}{g_m}} \right)^{g_m} \right]^2 \tag{7}$$

where g_α, g_n, g_c, g_l and g_m are material dependent fitting parameters and $S_e = \frac{S_{rw} - S_{res}}{S_{sat} - S_{res}}$ is the effective degree of liquid water saturation. S_{sat} and S_{res} are the maximum and minimum degrees of liquid water saturation, respectively. K_{sat} is the hydraulic conductivity when the water is fully unfrozen. Note that the degree of ice saturation S_{ice} is directly related to the degree of liquid water saturation by $S_{rw} + S_{ice} = 1$.

2.2 Energy balance equation

The thermal energy balance equation is expressed as [3]:

$$\rho c \frac{\partial T}{\partial t} + \rho_w c_w q_w \cdot \nabla T - L \rho_{ice} \frac{\partial \theta_{ice}}{\partial t} + \nabla \cdot (\lambda \nabla T) = 0 \tag{8}$$

The specific heat capacity ρc of the soil mixture is estimated as follows:

$$\rho c = \theta_s c_s \rho_s + \theta_w c_w \rho_w + \theta_{ice} c_{ice} \rho_{ice} \tag{9}$$

Here, θ_i represents the volume fraction of phase i, where $i = s, w$ or ice; s corresponds to solid particles, w to liquid water and ice to ice. The volume fraction of each phase is given by:

$$\theta_s = (1 - n);\ \theta_w = n S_{rw};\ \theta_{ice} = n(1 - S_{rw}) \tag{10}$$

The thermal conductivity λ of the mixture is assumed to be a function of the thermal conductivity of each phase scaled by its volume fraction:

$$\lambda = \lambda_s^{\theta_s} \lambda_w^{\theta_w} \lambda_{ice}^{\theta_{ice}} \tag{11}$$

The heat released during the phase change from liquid water to ice is captured by the middle term in Equation (8) through the inclusion of L, the latent heat of fusion. Note that:

$$\frac{\partial \theta_{ice}}{\partial t} = \frac{\partial [n(1 - S_{rw})]}{\partial t} = -\frac{\partial (n S_{rw})}{\partial t} = -\left(n \frac{\partial S_{rw}}{\partial t} + S_{rw} \frac{\partial n}{\partial t} \right) \tag{12}$$

Finally, rearranging Equation (8) gives:

$$\begin{aligned} \rho c \frac{\partial T}{\partial t} + \rho_w c_w q_w \cdot \nabla T + L \rho_{ice} n \frac{\partial S_{rw}}{\partial s_c} \frac{\partial s_c}{\partial T} \frac{\partial T}{\partial t} + \nabla \cdot (\lambda \nabla T) + L \rho_{ice} n \frac{\partial S_{rw}}{\partial s_c} \frac{\partial s_c}{\partial p_w} \frac{\partial p_w}{\partial t} \\ + S_{rw}(1 - n) \frac{\partial \varepsilon_v}{\partial t} = 0 \end{aligned} \tag{13}$$

For simplicity, in the current framework, the effect of the porewater pressure variation on cryogenic suction is neglected as well as the effect of volumetric change on the thermal flow.

2.3 Mechanical balance equation

The mechanical balance equation takes the form:

$$\nabla \cdot \boldsymbol{\sigma} + \mathbf{b} = \mathbf{0} \tag{14}$$

where $\boldsymbol{b}$ is the body force and the total stress $\boldsymbol{\sigma} = \boldsymbol{\sigma}' + S_{rw} p_w \mathbf{I}$ where $\boldsymbol{\sigma}'$ and $\mathbf{I}$ are the effective stresses and the identity tensor, respectively. The effective stresses are calculated as follows [4]:

$$\boldsymbol{\sigma}' = \mathbf{D}\left(\Delta \boldsymbol{\varepsilon} - \mathbf{m}^T \Delta \varepsilon_T - \mathbf{m}^T \Delta \varepsilon_{ph} \right) \tag{15}$$

Where $\mathbf{D}$ is the material stiffness matrix, $\Delta\boldsymbol{\varepsilon}$ is the total strain increment, $\mathbf{m}^T$ is the unity vector and $\Delta\varepsilon_{ph}$ is the strain increment due to phase change (ice to water and vice versa), and can be evaluated through the corresponding volumetric change $\Delta\varepsilon_{ph}^{vol}$ using the following formula:

$$\Delta \varepsilon_{ph} = \frac{1}{3} \Delta \varepsilon_{ph}^{vol} \Delta S_{ice} \tag{16}$$

with

$$\Delta \varepsilon_{ph}^{vol} = \frac{n(\rho_w - \rho_{ice})}{\rho_w S_{rw} + \rho_{ice} S_{ice}} \frac{dS_{ice}}{dT} \tag{17}$$

The thermal strain increment $\Delta\varepsilon_T$ is captured by the more common equation:

$$\Delta \boldsymbol{\varepsilon}_T = \alpha_T \Delta T \tag{18}$$

here α_T is the linear thermal expansion coefficient of soil. Furthermore, the stiffness is also updated based on the work by [4]. In fact, a detailed description of the mechanical model is not essential for the purpose of this study and is therefore omitted.

The above balance and constitutive equations were implemented into FEniCS-Geo [5], a fully coupled framework that works under FEniCS [6].

3 Slope stability calculations

The classical Limit Equilibrium Method was implemented within FEniCS-Geo finite element simulations to evaluate the slope safety factor at various stages of the freezing–thawing cycle. The stress field and ice content (related to the cryogenic suction) obtained from the THM calculations were used to estimate the safety factor. It was assumed that the internal friction angle φ' remains independent of ice content, while an additional contribution to cohesion is introduced with increasing ice content. A linear relationship between cryogenic suction and the additional cohesion is adopted [2], which leads to the following expression for the total cohesion c:

$$c = c' + k_{sc} s_c \tan \varphi' \tag{19}$$

where c' is the effective cohesion and k_{sc} is a parameter controls the increase of cohesion with cryogenic suction s_c. In this study the value of $k_{sc} = 0.1$ is adopted. Under low confining stresses, it is accepted that the linear relationship is reasonable at moderate subzero ranges, approximately 0 to −10 °C [7]. This allows for the direct implementation of the Limit Equilibrium Method (LEM) using the classical Mohr–Coulomb failure criterion to estimate the shear strength of frozen soil at a given degree of ice saturation (i.e. cryogenic suction) for a specified stress state. The calculations can then proceed in the usual manner, as in FEM-based LEM analyses [8]. In this study, 100 stress-sampling points along the assumed slip surface were used.

4 Numerical example

To assess the performance of the proposed framework, a synthetic slope is subjected to a freezing–thawing cycle over a period of ten days. The temperature varies between a maximum of +5 °C and a minimum of −5 °C. This temperature variation is applied as a thermal boundary condition at the top of the slope.

The slope geometry, finite element mesh, and boundary conditions are shown in Figure 1. The model parameters are summarized in Table 1and Table 2.

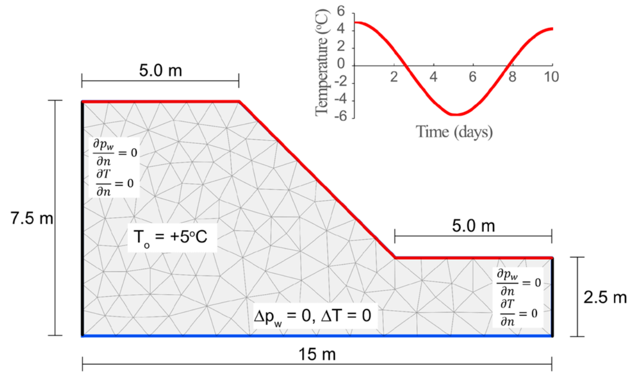

Figure 1. The Finite element model showing the geometry, FE mesh and boundary conditions.

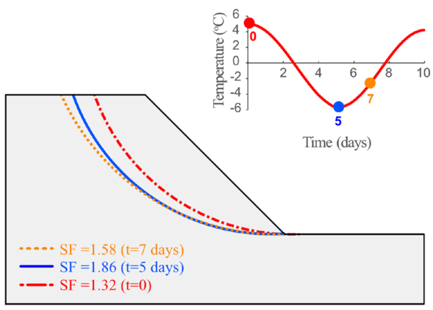

Figure 2. Calculated safety factor at t=0 and t=5 days.

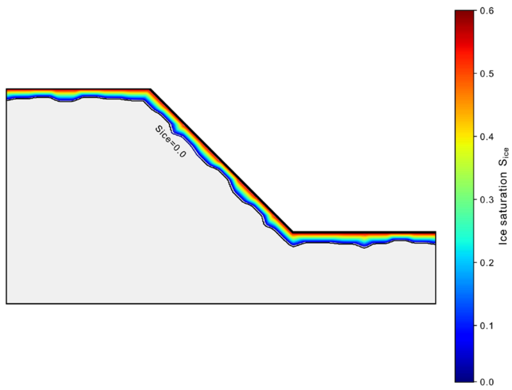

Figure 3. Colour map of ice saturation at t=5 day.

Table 1. Used parameters to model the curves of unfrozen water content and hydraulic conductivity.

Parameter	g_a	g_n	g_c	S_{sat}	S_{res}	g_m	g_l
Value	1E-7 (1/Pa)	2.5	-8.0	1.0	0.0	0.87	0.5

Table 2. THM model parameters.

Parameter	Symbol	Value	Unit
Internal friction angle	φ'	30	o
Effective cohesion	c'	5	kPa
Saturated hydraulic conductivity	K_{sat}	1E-8	m/s
Thermal conductivity of solid particles	λ_s	1.5	W/m/K
Thermal conductivity of water	λ_w	2.2	W/m/K
Thermal conductivity of ice	λ_{ice}	0.6	W/m/K
Specific heat capacity of solid particles	c_s	800	J/kg/K
Specific heat capacity of water	c_w	4190	J/kg/K
Specific heat capacity of ice	c_{ice}	2095	J/kg/K
Latent heat of fusion	L	333550	J/kg
Water compressibility	β_w	4.58E-10	1/Pa
Thermal expansion of water	β_{wT}	3.4E-4	1/K
Linear thermal expansion coefficient of solid particles	α_T	5E-6	1/K
Initial porosity	n	0.4	-
Density of solid particles	ρ_s	2600	kg/m^3
Density of water	ρ_w	1000	kg/m^3
Density of ice	ρ_{ice}	917	kg/m^3

5 Calculation results

Figure 2 shows the calculated initial safety factor at t = 0 and the evolution of the safety factor at t = 5 days (i.e. at the coldest time) and t = 7 days (i.e., during thawing). Furthermore, Figure 3 shows the predicted profile of ice saturation after 5 days. As expected, the safety factor increases due to the formation of a frozen layer at the top of the slope. In fact, the contribution of ice substantially increased the safety factor, despite the thin ice layer being less than 0.5 m, as shown in Figure 3. During thawing, the safety factor decreased as a result of the loss of additional cohesion.

In general, it is expected that the slope will exhibit a continuous reduction in safety factor with an increasing number of freezing–thawing cycles. During the freezing period, more water is attracted into the slope body, leading to a progressive increase in soil water content. This, in turn, results in elevated pore water pressure and a reduction in shear strength. In addition, variations in hydraulic conductivity within the thawing slope may lead to the development of localized regions of excess pore water pressure.

6 Conclusions

The current framework does not yet account for ice lens formation and segregation. Moreover, the employed mechanical model remains relatively primitive (i.e., nonlinear elastic) and is open to further development. Additionally, frozen slopes often exhibit more pronounced failure mechanisms [9], so the assumption of a simple circular slip surface represents a strong approximation in this case. Future work will address this limitation by employing more advanced slip-surface search methods. Finally, it is worth noting that the main objective of the present work is to establish a basic methodological framework, with subsequent efforts aimed at addressing the identified shortcomings.

References

1. S. Nishimura, A. Gens, S. Olivella, R. J. Jardine, THM-coupled finite element analysis of frozen soil: formulation and application. Géotechnique, **59**, no. 3, Art. no. 3 (2009)
2. Y. Lian, H. H. Bui, G. D. Nguyen, "A coupled THM-SPH computational framework for frozen soils and its applications for thawing-induced slope failure. Comput. Methods Appl. Mech. Eng., **446**, p. 118252 (2025)
3. H. R. Thomas, P. Cleall, Y.-C. Li, C. Harris, M. Kern-Luetschg, Modelling of cryogenic processes in permafrost and seasonally frozen soils. Géotechnique, **59**, no. 3, pp. 173–184 (2009)
4. Y. W. Bekele, H. Kyokawa, A. M. Kvarving, T. Kvamsdal, S. Nordal, Isogeometric analysis of THM coupled processes in ground freezing, Comput. Geotech., **88**, pp. 129–145 (2017)
5. A. Abed, E. Gerolymatou, M. Karstunen, FEniCS simulation of a partially saturated slope under varying environmental loads, in Proceedings 10th NUMGE 2023 (2023)
6. M. E. R. A. Logg K. B. Ølgaard, G. N. Wells, FFC: the FEniCS Form Compiler, in Automated Solution of Differential Equations by the Finite Element Method, vol. 84, K.-A. M. A. Logg, G. N. Wells, Eds., in Lecture Notes in Computational Science and Engineering, **84**, Springer (2012)
7. N. A. Tsytovich, The mechanics of frozen ground. McGraw-Hill Book Co. (1975).
8. D. G. Fredlund, R. E. G. Scoular, Using limit equilibrium concepts in finite element slope stability analysis. International Simposium on Slope Stability Engineering, pp. 31–47 (1999)
9. B. Ladanyi, O. Andersland, Frozen ground engineering. Wiley Hoboken (2004)